JOURNAL OF PROPULSION AND POWER
Vol. 21, No. 6, November–December 2005

Modeling of Hybrid Rocket Low Frequency Instabilities

M. Arif Karabeyoglu*
Stanford University, Stanford, California 94305
Shane De Zilwa†
NASA Ames Research Center, Moffet Field, California 94035
Brian Cantwell‡
Stanford University, Stanford, California 94305
and
Greg Zilliac§
NASA Ames Research Center, Moffet Field, California 94035

A comprehensive dynamic model of a hybrid rocket has been developed to understand and predict the transient behavior including instabilities. A linearized version of the transient model predicted the low-frequency chamber pressure oscillations that are commonly observed in hybrids. The source of the instabilities is based on a complex coupling of thermal transients in the solid fuel, the wall heat transfer blocking due to fuel regression rate, and the transients in the boundary layer that forms on the fuel surface. The oscillation frequencies predicted by the linearized theory are in very good agreement with 43 motor test results obtained from the hybrid propulsion literature. The motor test data used in the comparison cover a very wide spectrum of parameters including 1) four separate research and development programs; 2) three different oxidizers (liquid oxygen, gaseous oxygen, and nitrous oxide); 3) a wide range of motor dimensions, that is, from 5 in. (12.7 cm) diameter to 72 in. (182.9 cm) diameter, and operating conditions; and 4) several fuel formulations. A simple universal scaling formula for the frequency of the primary oscillation mode is also suggested.

Nomenclature

A	=	preexponential coefficient
A_p, A_n	=	port and nozzle throat areas
B	=	blowing parameter
C	=	specific heat of fuel
C_f, C_H	=	skin-friction coefficient and Stanton number
c'	=	boundary-layer delay time coefficient
c^*_{exp}, c^*_{theo}	=	measured and calculated characteristic velocities
D	=	average port diameter
E_a	=	activation energy
E_L, E_{E_a}	=	energy parameters
F_T	=	thermal system transfer function
F_{TC}	=	thermal–combustion coupled system transfer function
f, f_{1-L}	=	primary oscillation frequency, first acoustic mode frequency
G_o, G_t	=	oxidizer and total mass fluxes
$h_v L_v$	=	total and latent heats of gasification
$\hat{I}$	=	Laplace transform of oxidizer mass flux perturbation
k	=	blowing parameter exponent
L, L_m	=	length of the fuel port and motor
L^*	=	V_m/A_n
$\dot{m}_o$, $\dot{m}_t$	=	oxidizer and total mass flow rate
n	=	mass flux exponent
P_c	=	average chamber pressure
$\dot{Q}_c$, $\dot{Q}_w$	=	convective and total wall heat fluxes
$\dot{r}$, R	=	dimensional and nondimensional regression rate
Re_z	=	Reynolds number
$R_g R_u$	=	specific and universal gas constants
RT_{av}	=	average gas constant temperature product
s	=	Laplace transform variable
T	=	temperature
t	=	time
u, v	=	axial and normal velocities
U^*	=	diffusion speed
V_p, V_m	=	port and motor volumes
z	=	axial distance along the port
γ	=	ratio of specific heats
ΔP_{osc}	=	chamber pressure oscillation amplitude
δ	=	boundary-layer thickness
κ	=	thermal diffusivity of fuel
μ	=	average gas viscosity
ρ_f, ρ	=	fuel and average gas densities
σ_1, σ_2	=	gas-phase response coefficients
τ_{bl}, τ_{tl}	=	boundary layer response time and thermal lag time
τ_o	=	shear stress

Subscripts

a	=	ambient
e	=	freestream value
ref	=	reference quantities
s	=	surface
1	=	first perturbation variable

Superscripts

-	=	nondimensional variable
^	=	Laplace transform variable

Introduction

THE allowable thrust oscillations for an operational propulsion system are limited by certain practical considerations, including acceleration loads on the vehicle structures and also on the

Presented as Paper 2003-4463 at the Joint Propulsion Conference, Huntsville, AL, 20–23 July 2003; received 21 January 2004; revision received 25 February 2005; accepted for publication 25 February 2005.

*Senior Research Engineer, Department of Aeronautics and Astronautics. Member AIAA.
†National Research Council Postdoctoral Fellow. Member AIAA.
‡Professor, Department of Aeronautics and Astronautics. Fellow AIAA.
§Research Scientist. Member AIAA.

payload. This makes combustion stability a critical issue during the development of a new propulsion system. The combustion instabilities of solid and liquid systems have been studied in depth, and partially successful theories along with certain practical rules for designing stable systems have been developed.[1–3] Even with this extensive knowledge base, development of stable rocket systems requires a significant amount of time and resources during the design and testing phases of a program.

Although the transient operation and instability mechanisms of hybrids have not been explored as extensively as the more mature chemical systems, past experience shows that hybrids do not have the catastrophic instabilities that liquid and solid systems may potentially present. In fact, hybrid systems typically show finite amplitude, that is, 2–20% rms of mean chamber pressure, low-frequency chamber pressure oscillations.[4–8] This most common hybrid instability is in the form of limit-cycle oscillations with frequencies much smaller than the first longitudinal acoustic mode of the combustion chamber.

Even though the exact cause of the low-frequency hybrid instabilities is not yet known, a few plausible theories exist.[5,9–12] Most of the suggested theories lack the mathematical formalism that is commonly observed in the solid and liquid instability models. The fundamental difficulty in producing a mechanism that would generate instabilities comes from the fact that hybrid burn rates are typically independent of the chamber pressure. This, for example, eliminates the pressure coupling between the thermal lags in the solid and the chamber gasdynamics, which is the source of the L^* instabilities in solid rockets.[1]

One particular theory, the thermal–combustion (TC) coupled model,[13,14] which is based on the coupling of thermal lags in the solid and the transients in the gas-phase transport, has predicted (based on a mathematical formalism) fuel mass production oscillations that would drive the observed pressure oscillations. The purpose of this paper is to extend the TC coupled theory to include the effects of the chamber gasdynamics and compare the theory predictions with the motor test data. The merits and shortcomings of the extended TC coupled model will also be discussed.

Transient Phenomena in Hybrid Rocket Motors

Our approach to modeling the dynamic behavior of hybrids is to isolate the subsystems of the motor and consider every single subsystem individually. For a full description of motor transients one has to consider the following subsystems.

First is the feed system: In a hybrid motor, the liquid (or gaseous) oxidizer needs to be fed in to the combustion chamber through a feed system. In reality the feed system response time is finite due to the capacity of the elements in the system. Accurate response depends on the details of the system, which is likely to be significantly different for every design. For this reason, we will bypass the feed system dynamics in our investigations by assuming the oxidizer mass flow rate as the input parameter. This is a reasonable assumption for most systems because isolating elements, that is, cavitating venture, sonic orifice, are present.

Vaporization of the liquid oxidizer is the second subsystem. Complete vaporization of the oxidizer droplets in the combustion chamber requires a certain characteristic time depending on parameters such as the droplet size and the thermal/flow environment of the space where droplet vaporization takes place. For the purposes of this paper we will assume that the oxidizer is in gaseous phase when it enters the port.

Diffusion and combustion in the boundary layer comprise the next subsystem. It requires some time for the hybrid boundary-layer properties to adjust to the changes in the port velocity or the fuel blowing from the surface. The associated dynamics has been discussed in detail in Refs. 13 and 14 and will be briefly covered later in this paper.

Thermal response in the solid grain is the fourth subsystem. A change in the wall heat flux to the hybrid fuel grain can not be followed immediately by fuel production due to the finite heat capacity of the solid fuel.

The chamber gasdynamics is the last subsystem. The chamber pressure responds to the changes in the mass flow with a timescale proportional to the filling time of the chamber. Acoustic response is also resolved in this subsystem.

In the subsequent sections, the last three of these subsystems will be modeled and investigated individually. Eventually, these subsystems will be coupled to give the overall system response. The order of magnitude estimates of the timescales of some of the important processes encountered in a typical hybrid motor are listed in Table 1. In our modeling, solid and gaseous kinetic times are assumed to be fast compared to the other relevant timescales.

Thermal Lag Model

The regression rate of the hybrid fuel grain cannot respond to the changes in the surface heat flux instantaneously due to the finite thermal conductivity of the solid fuel. A complete transient model for a hybrid rocket system requires a dynamic model to predict the regression rate history for a given wall heat flux schedule. To serve this purpose, a thermal lag model that models the nonlinear heat conduction in the fuel grain with a moving boundary has been formulated and reported in Refs. 13 and 14. The schematic of this particular model is shown in Fig. 1.

In the thermal lag model, the gasification and pyrolysis reactions at the surface are both modeled by an exponential expression of the Arrhenius type. For chemical reactions, the exponential constant is an activation energy, whereas in vaporization it is the latent heat. To describe this behavior, we assign an average effective activation

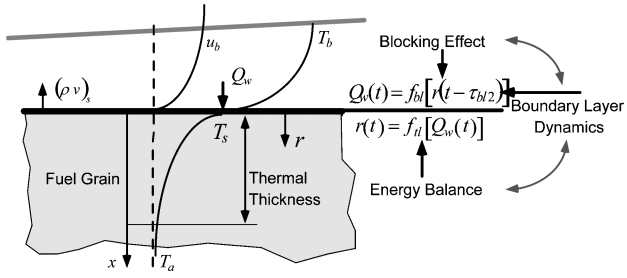

Fig. 1 Thermal lag model and TC coupling mechanism.

Table 1 Transient timescales of various phenomena in typical hybrid rocket

Physical phenomenon	Timescale	Explanation
Solid-phase kinetic times, s	$\tau_{sp} < 10^{-3}$	Degradation mechanisms of the polymer
Gas-phase kinetic times, s	$\tau_{gp} < 10^{-3}$	Hydrocarbon combustion mechanisms
Feed system response times	Varies greatly from system to system	Response time of the feed system
Evaporation times	$\tau_{\text{evap}} = f(U_o, T_1, \Delta P)$	Evaporation process of the liquid oxidizer
Thermal lags in solid, s[a]	$\tau_{\text{tl}} \propto \kappa/r^2 \approx 10^{-1}$	Thermal profile changes in the solid grain
Boundary-layer diffusion times, s[a]	$\tau_{\text{bl}} \propto L/u_e \approx 10^{-1}$[b]	Turbulent boundary layer diffusion processes
Acoustic times (longitudinal), s[a]	$\tau_a \propto L/c \approx 10^{-3}$[b]	Propagation of the acoustic waves
Gasdynamic filling times, s[a]	$\tau_{\text{fill}} \propto L^*/c^* \approx 10^{-1}$[b]	Global mass flow balance

[a]Modeled herein. [b]Varies greatly from case to case.

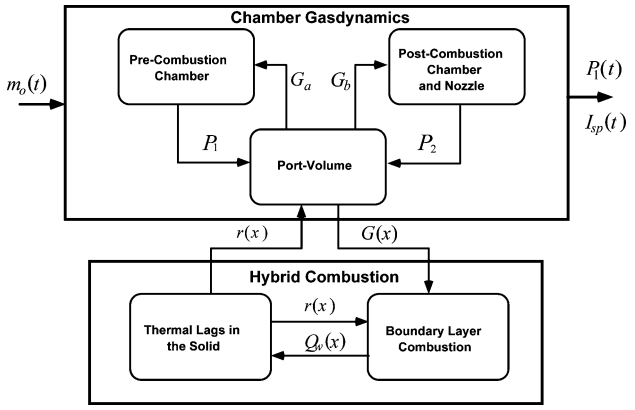

Fig. 2 TCG coupled system.

energy E_a, resulting in

$$\dot{r} = A \exp(-E_a / R_u T_s) \tag{1}$$

where T_s is the surface temperature. The mathematical formulation and various solution techniques for the thermal lag model are presented in Ref. 13. One solution of interest is obtained by perturbing the full nonlinear system around the nominal operating point. The linear initial boundary-value problem defined for the first-order perturbation quantities has been solved with use of the Laplace transformation technique. In this case, the transfer function between the regression rate perturbation and the applied heat flux perturbation can be written as

$$F_T = \frac{\hat{R}_1(s)}{\hat{Q}_1(s)} = \frac{2E_{E_a} s}{\left(1 + \sqrt{4s+1}\right)\left(s + E_{E_a}\right) - 2E_{E_a} + 2E_L E_{E_a} s} \tag{2}$$

Note that $\hat{R}_1(s)$ and $\hat{Q}_1(s)$ are the Laplace transforms of the nondimensional regression rate perturbation and the wall heat flux perturbation, respectively. The following nondimensional parameters are defined for convenience:

$$E_{E_a} = E_a \Delta T \Big/ R_u (T_s)^2_{\text{ref}}, \qquad E_L = L_v / C \Delta T$$

$$\Delta T = (T_s)_{\text{ref}} - T_a, \qquad \bar{Q} = \dot{Q}_w / \dot{Q}_{\text{ref}}$$

$$R = \dot{r} / \dot{r}_{\text{ref}}, \qquad \dot{Q}_{\text{ref}} = \dot{r}_{\text{ref}} \rho_f C \Delta T$$

The reference state indicated by subscript ref corresponds to the nominal operating point around which the system is perturbed.

Equation (2) relates the wall heat flux to the regression rate in the Laplace space and establishes one block in our overall transient model that is shown schematically in Fig. 2. Various important characteristics of a linear system including stability can be inferred from the denominator of its transfer function commonly referred as the characteristic equation. This transfer function for the thermal system, which contains a square root term, produces a phase lead between the heat flux and the regression rate in the low end of the frequency domain.[13] As will be discussed in the following sections, this phase lead capability will play a critical role in the production of low-frequency instabilities.

Gas-Phase Combustion Model

In the thermal lag model, we have treated the surface heat flux as a parameter that can directly be controlled. However, in a hybrid motor, the oxidizer mass flow rate is the primary input variable that can be easily changed by the action of a valve. The actual response of the motor to a change in the oxidizer mass flow is rather complicated during a transient. As the oxidizer mass flow rate of the motor changes, the mass flux at a characteristic point in the port reacts to the change as does the turbulent boundary layer developed over the fuel surface. In this section, we will summarize the modeling of the boundary-layer combustion dynamics and investigate its interactions with the thermal lags in the solid. For the sake of simplicity, we will ignore the radiative heat transfer to the fuel surface, which is typically a relatively small fraction of the total heat flux. Unless the radiation dominates the convection component of the surface heat transfer, the transient model developed in this paper is expected to be valid.

In our preliminary model, we assume that the boundary-layer response is quasi-steady, namely, the boundary-layer diffusion lag times are small compared to the thermal lag times in the solid. Under the quasi-steady assumption, one can use the classical approach[15] to calculate the response of the wall heat flux to the changes in mass flux. However, the results of classical hybrid theory cannot be used directly during a transient in the solid because the convective heat transfer to the wall depends explicitly on the instantaneous regression rate through the blocking generated by the blowing of the gaseous fuel from the surface. In the presence of the thermal lags, the blocking generates a coupling mechanism in the gas phase between the regression rate and the heat flow to the surface. Based on this understanding, the classical theory can be modified to obtain a functional relation between wall heat flux and oxidizer mass flux-regression rate combination in terms of nondimensional parameters:

$$\bar{\dot{Q}}_c(\bar{t}) = E_L \bar{G}_o^{n/(1-k)} R^{-k/(1-k)} \tag{3}$$

Note that $\bar{G}_o = G_o/(G_o)_{\text{ref}}$, $\bar{\dot{Q}}_c = \dot{Q}_c/\dot{Q}_{\text{ref}}$, n is the oxidizer flux exponent, and k is the blowing correction exponent first defined by Marxman, that is, $C_H/C_{Ho} = B^k$. Here the local total mass flux that appears in the original Marxman formulation is replaced by the oxidizer mass flux for convenience. The justification for that transformation is given in Ref. 14.

Thus far in the development of the transient hybrid combustion theory, we assumed that the boundary layer responds rapidly to the changes in the mass flux compared to the other transient timescales in the rocket motor such as the gasdynamic lags or the thermal lags. This assumption fails to be valid especially for large hybrid motors. To develop a realistic model for the dynamics of the hybrid motor, the boundary-layer lags must be considered. Because this complex dynamic phenomenon is extremely difficult to investigate both theoretically and experimentally, we consider the simpler cases reported in the literature of an incompressible turbulent boundary layer with no blowing or chemical reactions.[16] The most important conclusion for this simplified case is that the time required for transition from the initial equilibrium profile to the final equilibrium profile at any axial location z is proportional to the time of flight of a fluid particle from the leading edge of the boundary layer to the specific axial location at the speed of the freestream flow, u_e. This very important result can be formulated for hybrid boundary layers as

$$\tau_{\text{bl}} = c'(z/u_e) \tag{4}$$

Here c' is a constant that needs to be determined empirically. We will call this time required for equilibration the characteristic response time of the boundary layer, τ_{bl}. Note that the physical nature of the boundary-layer transient time is not related to the propagation of the disturbances with the speed of the port velocity as suggested by Eq. (4). The delay, rather, depends on the diffusion timescale across the boundary layer, which is proportional to the ratio of the local boundary-layer thickness to the diffusion speed, $\tau_{\text{bl}} \cong \delta/U^*$. The diffusion speed is defined in terms of the shear stress and mean gas density as $U^* = \sqrt{(\tau_o/\rho)}$. The boundary-layer delay time, after the substitution of the standard (incompressible) turbulent boundary-layer expressions[17] for the shear stress, $\tau_o = 0.0288 \rho u_e Re_z^{-0.2}$, and the thickness, $\delta = 0.37 z Re_z^{-0.2}$, becomes $\tau_{\text{bl}} = 2.18 Re_z^{-0.1} z/u_e$. Here the local Reynolds number is defined as $Re_z = u_e z \rho/\mu$. Note that the coefficient c' is found to be a weak function of the local Reynolds number. Thus, for simplicity, we assume that c' is constant. For Reynolds numbers corresponding to typical hybrid operation, c' is estimated to be approximately 0.55. In a real hybrid boundary layer with combustion and blowing, c' can be different from this estimation, and for that reason, it is determined empirically.

For the purpose of this paper, it is convenient to consider an average boundary-layer delay and replace the local distance z with the half of the grain length, $L/2$. Note that the empirical constant c' accounts for the correction to the inaccurate selection of the length scale L. However, we recognize that in reality there is a range of boundary-layer delay times that should be considered. Thus, the significant observation here is that a relatively broadband of oscillation frequencies is expected as opposed to a very sharp peak at the center frequency corresponding to $L/2$.

In our studies, the response of the boundary layer to the changes in the mass flux is accounted for by simply inserting time delays in the heat-flux expressions derived under the assumption of quasi-steady response. The implementation of this idea in the linearized version of Eq. (3) yields

$$\bar{Q}_1(\bar{t}) = \sigma_2 \bar{G}_1(\bar{t} - \bar{\tau}_{\mathrm{bl1}}) - \sigma_1 R_1(\bar{t} - \bar{\tau}_{\mathrm{bl2}}) \tag{5}$$

where

$$\bar{t} = t/\tau_{\mathrm{tl}}, \qquad \bar{\tau}_{\mathrm{bl1}} = \tau_{\mathrm{bl1}}/\tau_{\mathrm{tl}}, \qquad \bar{\tau}_{\mathrm{bl2}} = \tau_{\mathrm{bl2}}/\tau_{\mathrm{tl}}$$

$$\sigma_1 = (E_L + 1)[k/(1-k)], \qquad \sigma_2 = (E_L + 1)[n/(1-k)]$$

and $\tau_{\mathrm{tl}} = \kappa/\dot{r}^2$.

Here τ_{bl1} and τ_{bl2} are the time delays experienced by the wall heat flux $\dot{Q}_c$ to the changes in the oxidizer mass flux and the regression rate, respectively. The scaling of the time delays τ_{bl1} and τ_{bl2} obey the general scaling law given by Eq. (4). However the c' coefficients for τ_{bl1} and τ_{bl2} are expected to be different because each of these delays represents a different adjustment mechanism for the boundary layer. The model presented by Eq. (5) is central to the analysis in that it relates the heat conduction in the solid to the boundary-layer combustion.

TC Coupled System

Now, with the use of Eq. (5), the thermal lags in the solid can be coupled to the combustion transients in the boundary layer. This coupling yields the following transfer function between the oxidizer mass flux $\hat{I}(s)$ and the regression rate $\hat{R}_1(s)$ and represents the hybrid combustion block in the overall transient model (Fig. 2),

$$F_{\mathrm{TC}}(s) = \frac{\hat{R}_1(s)}{\hat{I}(s)} = \frac{2E_{E_a}\sigma_2 e^{-\bar{\tau}_{\mathrm{bl1}}^{s}s}}{\left(1+\sqrt{1+4s}\right)\left(s+E_{E_a}\right) - 2E_{E_a} + 2E_{E_a}s\left(E_L + \sigma_1 e^{-\bar{\tau}_{\mathrm{bl2}}s}\right)} \tag{6}$$

This transfer function (TC coupled system) that represents the combustion phenomenon includes the dynamics of the thermal processes in the solid and approximates the combustion dynamics in the turbulent boundary layer of the rocket motor. Equation (6) can be used to investigate the stability character of the TC coupled system. The commonly used method is to map the poles of the transfer function in the s plane. Particularly, the real component of a certain pole of a transfer function indicates amplification rate associated with that pole. Similarly the imaginary part represents the oscillation frequency.

First a system with zero boundary-layer delays, that is, $\tau_{\mathrm{bl1}} = \tau_{\mathrm{bl2}} = 0$, is determined to be always stable. In fact, Fig. 3, which is the transfer function for a system with typical parameters, shows no poles in the s plane [only a zero at (0, 0)], indicating no sign of instability. If a positive delay is introduced between the regression rate and wall heat flux, a series of unstable poles is generated. The example case with a 38-ms-delay is shown in Fig. 4. Note that all of the other parameters are kept identical to the case with no delays. Even though there exists an infinite series of poles generated (at the same amplification rate), we will only concentrate on the pole with the lowest frequency (fundamental mode). We believe that the higher-order modes are an artifact of using a simple delay instead of the full dynamics for the boundary-layer transients. Moreover, the higher frequency modes, even if they exist in a real system, are likely to be damped more effectively compared to the fundamental mode.

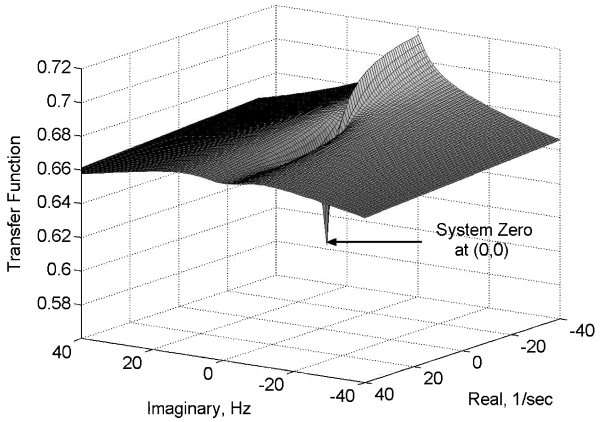

Fig. 3 Transfer function of TC coupled system with no delays ($\tau_{\mathrm{bl1}} = \tau_{\mathrm{bl2}} = 0$): HTPB system with $E_a = 15$ kcal/mole.

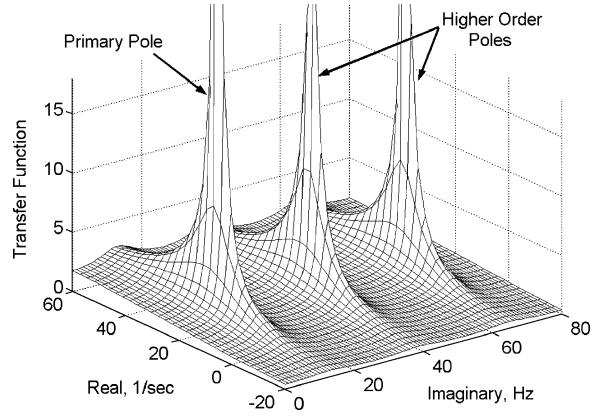

Fig. 4 Unstable poles of TC coupled system in s plane for $\tau_{\mathrm{bl1}} = 0$ and $\tau_{\mathrm{bl2}} = 38$ ms: HTPB system with $E_a = 15$ kcal/mole.

It is important to identify the necessary conditions that must exist for the generation of TC coupled instabilities. A careful examination of the denominator of the transfer function, Eq. (6), shows that for the instability to exist blowing exponent k, activation energy E_a, and delay time τ_{bl2} must be nonzero. This indicates that the instability is a result of the coupling of three physical phenomena: blocking of heat transfer by radial injection of fuel mass, thermal transients in the solid and boundary-layer dynamics. The gas-phase/solid-phase coupling mechanism captured by the TC coupled model is shown in Fig. 1.

Next we consider the effect of various parameters on the TC coupled instability. It can be shown that the effect of the regression rate mass flux exponent n, the heat of vaporization of the fuel, L_v the heat capacity of the solid fuel, C, and the surface temperature T_s on the oscillation frequency and amplitude is negligible for the range of these parameters that are commonly found in hybrid systems. Also TC coupled system characteristics are completely independent of the solid density ρ_f and the heat diffusivity in the solid, κ.

The effect of the activation energy on the amplification, and frequency is shown in Fig. 5 for $\tau_{\mathrm{bl2}} = 38$ ms and $k = 0.68$. As indicated by Fig. 5, for activation energies commonly observed in hybrids, ranging from 5 to 60 kcal/mole, the variation in the oscillation frequency is relatively small. The amplification increases with increasing activation energy. For this specific case, the systems with activation energies larger than 3 kcal/mole show positive amplification and unstable behavior. Decreased stability at higher activation energies is expected because at high E_a values the surface temperature and regression rate are more closely coupled. This coupling is one of the necessary ingredients for the generation of the

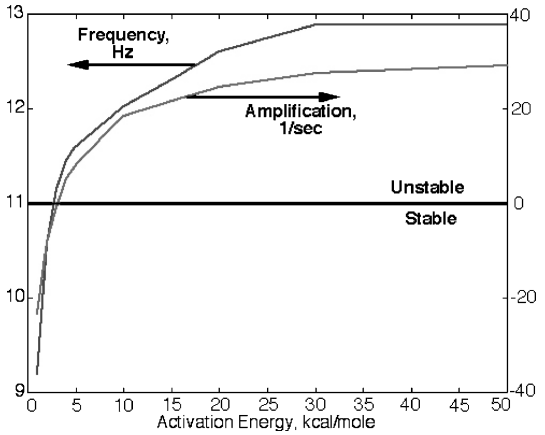

Fig. 5 Effect of activation energy on oscillation frequency and amplification.

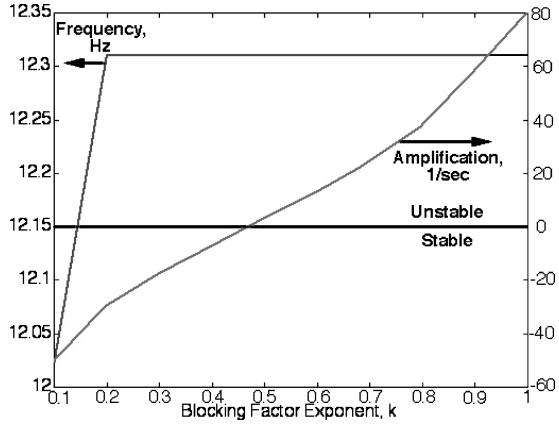

Fig. 6 Effect of blocking factor exponent on oscillation frequency and amplification.

instabilities. In fact in the extreme case of $E_a = 0$, for which the surface temperature is completely independent of the regression rate, oscillation frequency goes to infinity and the amplification asymptotes to negative infinity.

The activation energies for the polymeric systems that are typically used in hybrids range from 10 to 60 kcal/mole. If the thermal degradation reactions can be ignored, the activation energy for the nonpolymeric paraffin-based fuel system would be equivalent to the latent heat of vaporization.[18] This value for the paraffin-based fuel formulations is estimated to be 17 kcal/mole (Ref. 13). If the surface temperature of a paraffin-based fuel is dictated by the pyrolysis reactions as opposed to the phase change, the activation energy can be assumed to be approximately 60 kcal/mole. In either case, the activation energy is high enough such that the stability character is not affected.

Similar results can be obtained for the effect of the blocking exponent, as shown in Fig. 6 for $\tau_{bl2} = 0.38$ and $E_a = 15$ kcal/mole. For the range of values reported in the literature for k, that is, 0.68–0.77 (Refs. 15 and 19), the effect of blowing exponent on the frequency is negligible. The amplification increases with increasing k, and systems with k values 0.45 and larger showed unstable behavior. Note that for the physically unrealizable case of $k = 0$ the instability disappears because one of the necessary coupling mechanisms is eliminated. Finally note that, even though the blocking effect in paraffin-based systems is somewhat reduced due to the two-phase character of the flowfield, it is still significant enough to establish the coupling between the gas phase and solid phase.

The most influential parameter on the TC coupled frequency is determined to be the boundary delay time τ_{bl2}. Figure 7 shows the predicted frequency as function of the delay time for three activation energy values, $E_a = 5$, 15, and 50 kcal/mole. As shown in Fig. 7, the

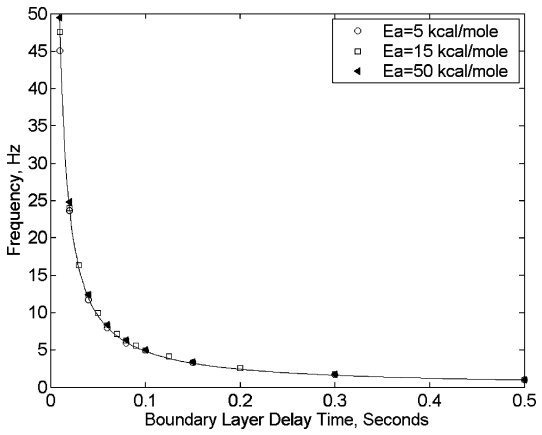

Fig. 7 Effect of boundary-layer delay time on oscillation frequency for various activation energies.

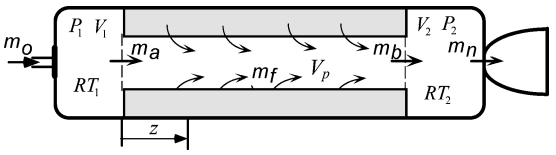

Fig. 8 Schematic of 2V-port model.

effect of the activation energy on the frequency, especially at longer delay times, is small. For the purposes of this paper, the effects of activation energy and blowing exponent will be ignored and the frequency will be represented as a function of the boundary delay time alone. The following curve-fit equation is suggested to quantify the inverse relationship between the frequency and the boundary-layer delay time:

$$f = 0.48/\tau_{bl2} \tag{7}$$

As shown in Fig. 7, this expression represents the predicted frequency to a very high degree of accuracy and will be used for all of the hybrid systems that will be discussed later in this paper.

Gasdynamic Model

In the preceding section, the dynamic models for the thermal lags and the hybrid combustion are summarized. In addition, these subsystem models are coupled to obtain the response of the fuel mass generation to the changes in the mass flux in the port. However, practically significant parameters of the rocket operation such as the chamber pressure, specific impulse, and thrust cannot be obtained solely from the TC coupled system. These variables can only be determined after introducing a model for the gasdynamics, which will be discussed in this section. A gasdynamic model, in general, should use the oxidizer mass flow rate and the fuel mass generation rate as the inputs, and it should yield the parameters that are more closely related to the performance of the motor such as the chamber pressure and the motor oxidizer to fuel ratio (O/F) as the outputs.

A specific gasdynamic model (2V-port model) has been developed in Refs. 13 and 20. In this particular model, the chamber has been divided into three components, precombustion chamber, fuel port volume, and postcombustion chamber (Fig. 8). The pre- and postcombustion chambers have been treated as zero-dimensional volume elements, but the variation of state variables along the axis of the fuel port has been taken into account. The mathematical formulation has been obtained after the application of the conservation laws for the three volume elements. The set of equations resembling our model has been solved analytically after linearization, and as a result of that operation, a transfer function for the gasdynamic subsystem has been obtained. Some numerical simulations are also performed based on the 2V-port model to validate of the approximations used in the perturbation solutions.

Table 2 Estimated and observed longitudinal acoustic frequencies for AMROC DM-01 motor

Longitudinal acoustic mode	Estimated (isothermal) frequency, Hz	Corrected frequency, Hz	Observed frequency, Hz	Estimated amplification, 1/s
First	48.4	53.0	50–55	−22
Second	96.7	103.9	100–110	−22
Third	142.6	156.1	150–165	−21
Fourth	191.1	209.3	200–220	−19
Fifth	240.7	263.6	250–275	−18

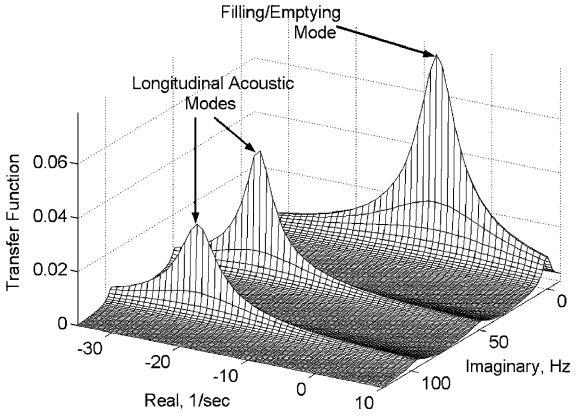

Fig. 9 Transfer function for pure gasdynamic system.

The following conclusions can be drawn from the results of the gasdynamic model as given in detail in Ref. 13 and 20.

1) The gasdynamic model captures the filling/emptying dynamics and also the longitudinal acoustic response of the hybrid combustion chamber. As can be seen from Fig. 9, acoustic modes are stable (well damped). No unstable oscillation modes are generated by the gasdynamic system by itself.

2) The nonlinear disturbances excite the chamber acoustic modes. Simulations showed that a sudden pulse in the oxidizer mass flow rate excites the acoustics modes. These modes decay in a relatively short period. This ringing phenomenon shows that the longitudinal acoustic modes can be driven by nonlinear low-frequency oscillations. Namely, the nonlinear low-frequency pressure waveforms continuously excite the acoustic modes of the chamber. An American Rocket Company (AMROC) motor DM-01 showed at least five longitudinal acoustics modes. All of those were well damped. The gasdynamic model, when corrected for isentropic speed of sound, predicts the acoustics frequencies of the DM-01 motor to a high level of accuracy (Table 2).

3) The gasdynamic model coupled with the boundary-layer dynamics ($\tau_{bl1} \neq 0$) does not produce any instabilities. (No extra poles are generated in the s plane.) This conclusion is based on transfer function analysis and also numerical simulations. This important result highlights the importance of the thermal lag system, that is, its unique dynamic capability of producing a phase lead, in producing a coupling mechanism to generate low-frequency unstable modes.

TC–Gasdynamic-Coupled System

In this section we integrate the gasdynamic system to the TC-coupled system to establish the TC–gasdynamic (TCG)-coupled response (Fig. 2). The TCG coupled system yields the performance of the rocket (such as chamber pressure) for some given input of oxidizer mass flow rate, which is a fundamental control parameter in hybrid rockets. It is fair to state that the TCG-coupled system represents the most fundamental dynamic behavior of a hybrid rocket.

The schematic of the hybrid subsystems and the information flow between the subsystems in the context of TCG coupling are shown in Fig. 2. Note that the lower block in the schematic represents the TC-coupled system. The input for the TC-coupled system is the local mass flux information, and the output is the mass generation or the regression rate. The upper block shows the 2V-port gasdynamic model. The gasdynamic model takes the oxidizer flow rate and the mass generation rate information and reveals the important performance parameters such as the chamber pressure and specific impulse. The TCG-coupled system can be considered as an overall model for the dynamics of a hybrid propulsion system that uses gaseous oxidizer, which is delivered by an isolated feed system.

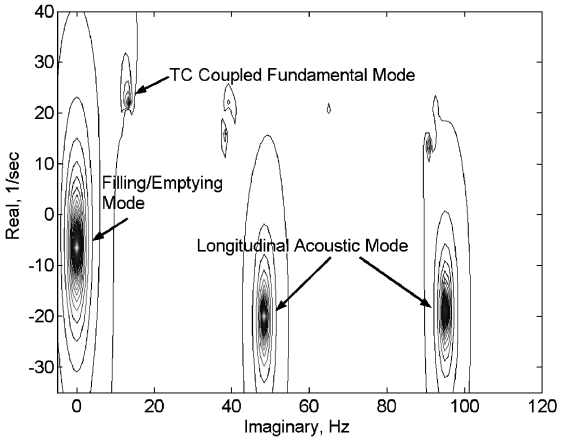

Fig. 10 TCG coupled system with $\tau_{bl2} = 38$ ms: most transient features of hybrid system deduced from locations of poles.

The generalization of the TCG-coupled system to a liquid hybrid with significant feed system dynamics can be achieved easily. Namely, two more modules for the liquid droplet evaporation and the feed system dynamics must be added to the front end of the TCG model. We believe that the fundamental phenomenon generating the common low-frequency instabilities of hybrid systems does not involve either of the evaporation lags or the feed system dynamics. However, we must state that liquid-fed hybrid systems, especially the cryogenic liquid oxygen systems, showed instabilities induced by the finite vaporization lags of the injected oxidizer. These type of instabilities are distinct from the commonly observed low-frequency instabilities that are produced by the TC coupling.

In the TCG-coupled system, the gasdynamic module converts the fuel mass oscillations produced by the TC-coupled system into the chamber pressure oscillations. It has been determined that, in the process of conversion, the oscillations produced by the TC-coupled system, that is, frequencies and amplification rates, are not altered. This fact is demonstrated in Fig. 10, which shows the TCG system transfer function for the TC-coupled system shown in Fig. 4. Figure 10 also indicates poles associated with the filling/emptying mode (first-order nonoscillatory mode) and the longitudinal acoustic modes with negative real components (damped). TCG coupled system captures all of the necessary underlying dynamics (linearized version) of a gaseous hybrid with a decoupled feed system.

NASA Ames Research Center Paraffin-Based Motor Tests

A promising fast burning, paraffin-based fuel has been tested extensively in the Hybrid Combustion Facility (HCF) at NASA Ames Research Center.[21] The motor outside diameter is 10 in., and gaseous oxygen is the oxidizer for all of the tests conducted at the HCF. The pressure time trace of a typical paraffin-based hybrid motor test is shown in Fig. 11, whereas the Fourier transform for the same test is given in Fig. 12. Note that the chamber pressure traces for classical hybrids as presented in the literature are very similar in nature. As indicated in Fig. 11 for a particular case, the feed system and the chamber were completely decoupled for all paraffin-based motor tests used in this paper.

The Fourier transform shows three broad peaks corresponding to the low-frequency hybrid instability, the Helmholtz mode, and the first longitudinal mode. It has been generally observed that the dominant mode, low-frequency oscillations are accompanied by lower amplitude higher frequency acoustic modes. See Ref. 6 for an extensive discussion of the stability characteristics of the paraffin-based motors.

Table 3 Parameters used in frequency estimations for AMROC motors

AMROC motor (thrust, lb)	O/F	c^*_{theo}, ft/s	c^*_{exp}, ft/s	L^*, in.	f, Hz	τ_{bl2}, m
S motor (10,000)	1.45	5584	5361	570	11	40.6
Half scale (33,000)	1.45	5584	5361	1305–1430	4.8	97.5
H-500 (75,000)	1.45	5584	5361	1770–2340	4.0	146.3
DM-01 (250,000)	1.55	5700	5472	2168	2–3.5	156.0

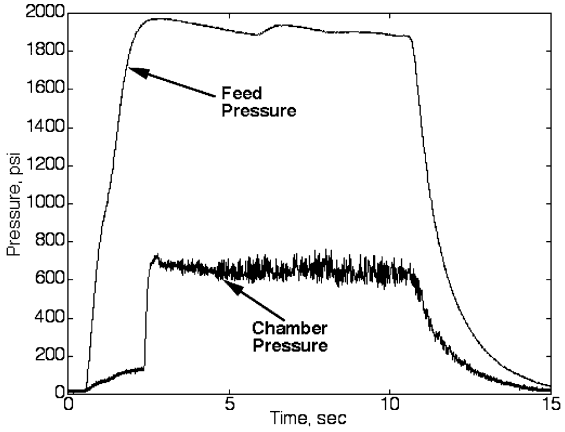

Fig. 11 Chamber and feed pressure time traces for paraffin-based motor test, 4L-05.

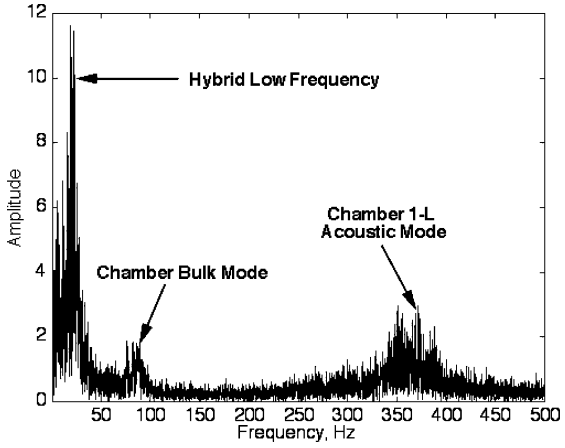

Fig. 12 Fourier transform of chamber pressure for the paraffin-based motor test, 4L-05.

Comparison of Theory Results with the Motor Test Data

In this section, we will compare the TCG coupled theory oscillation frequency predictions with the chamber pressure oscillation frequencies from hybrid motor test data. To produce a conclusive comparison, we have selected a large number of tests from several hybrid rocket development programs. The key features of each program is discussed briefly in the following paragraphs.

1) In the AMROC motor tests[4,13] case, the reported results are for four different thrust-class hybrid motors, which all used liquid oxygen (LOX) gaseous oxygen (GOX) as the oxidizer and hydroxyl-terminated polybutadiene (HTPB) as the fuel. The data from the AMROC tests are given in Table 3.

2) For the hybrid propulsion demonstration program (HPDP) 11-in. motor tests,[5,8] the oxidizer used is LOX and GOX and the fuel is an HTPB/Escorez formulation. The motor case diameter was 11 in. and the data from five tests used in this study are given in Table 4. Only the tests that exhibit combustion instability and performed with single-port motors are considered. The runs with the rearward-facing steps at the port entrance are also excluded in this study because in these tests the flowfield in the port is significantly altered, which may cause a major change in the boundary-layer delay time coefficient. We also include test 1 of 11-in. LOX motor data in the analysis. We only consider test 1 because it is the only run with a chamber configuration identical to GOX motors used in the calculations.

3) For the Joint Independent Research and Development Group (JIRAD) motor tests,[13,22] the oxidizer used is GOX and the fuel is an HTPB/Escorez formulation. The motor case diameter was 11 in., and the data from eight tests used in this study are given in Table 5. Only the tests that exhibit combustion instability and performed with single-port motors are considered here.

4) One test at Arizona State University[23] is included in the comparison for a 5-in.-diam nitrous oxide motor. The fuel was HTPB, see Table 6.

5) The paraffin-based motor tests[21] are conducted at NASA Ames Research Center in a 10-in.-diam test facility. The oxidizer was GOX, and the fuel is two separate nonpolymeric paraffin-based formulations. The data from 25 motor tests are reported in Table 7.

The prediction of the frequency requires the estimation of the boundary-layer delay time for each test from the reported data. Because the reported data are somewhat different for each program, different scaling laws for the delay time must be derived.

The first one is for the various size AMROC motors, which operated at different L^* levels. Because the information on the AMROC motors that can be found in the literature is limited to L^*, c^*, and motor O/F, it is desirable to express the boundary-layer delay time [Eq. (4) with $z = L/2$] in terms of those variables. The average velocity in the port can be approximated as

$$u_{av} = \frac{G_t[(1 + 2\text{O/F})/(1 + \text{O/F})]RT_{av}}{2P_c} \tag{8}$$

where RT_{av} is an average value in the port. Substituting this expression in the delay formula and using the relations for the total mass flow rate $\dot{m}_t = G_t A_p$ and port volume $V_p = LA_p$ yields

$$\tau_{bl2} = c' \frac{V_p P_c}{\dot{m}_t[(1 + 2\text{O/F})/(1 + \text{O/F})]RT_{av}} \tag{9}$$

With the use of the total mass flow relation, $\dot{m}_t = P_c A_n / c^*_{exp}$, and the definition $L^* = V_m / A_n$, the delay equation can be written as

$$\tau_{bl2} = c' \frac{V_p}{V_m} \frac{[(1 + \text{O/F})/(1 + 2\text{O/F})]}{RT_{av}} L^* c^*_{exp} \tag{10}$$

Here V_p/V_m is the ratio of the port volume to the motor volume, which is estimated to be approximately 0.85 for AMROC DM-01 motor. We assume that all AMROC motors possess the same average gas constant temperature product RT_{av} and volume ratio V_p/V_m. After it is noted that all motors operate at very similar O/F ratios and c^*_{exp} values, it can be stated that in this series of tests the boundary-layer characteristic delay time is proportional to L^*.

To reduce data from the rest of the tests, a similar relation for the boundary-layer delay time in terms of the chamber pressure and port flux levels must be derived. The port velocity can be replaced by an average value $(G_o + G_t)/2\rho_{av}$ with ρ_{av} given by the gas law $P_c = \rho_{av} RT_{av}$ to yield, finally, for the boundary-layer lag

$$\tau_{bl2} = c'[LP_c/(G_o + G_t)RT_{av}] \tag{11}$$

Equation (11) gives the scaling law for the boundary-layer delay in terms of the operating points of the rocket motor and also with the size of the motor. This states that delay increases with increasing chamber pressure and port length and decreases with increasing mass flux in the port. An important conclusion that can be drawn from those observations is that an increase in the chamber pressure or a decrease in the port mass flux acts to decrease the oscillation frequency of this type of TC coupled system.

The total mass flux can be eliminated form Eq. (11) by introducing the average O/F of the motor,

$$\tau_{bl2} = c' \left[LP_c \Big/ \left(2 + \frac{1}{\text{O/F}} \right) G_o RT_{av} \right] \tag{12}$$

Equation (12) will be used to reduce the paraffin-based motor data.

Table 4 Parameters used in frequency estimations for 11-in. hybrid motor tests[a]

Test	$\bar{D}$, in.	$\dot{m}_o$, lb/s	G_o, lb/in.$^2\cdot$ s	G_t, lb/in.$^2\cdot$ s	P_c, psi	O/F	f, Hz	ΔP_{osc}, psi	τ_{bl2}, ms
1 (GOX)	4.25	6.0	0.423	0.571	600	2.85	13	200	49.3
2 (GOX)	4.25	5.7	0.402	0.541	550	2.89	8	300	47.6
7 (GOX)	4.20	4.7	0.339	0.458	440	2.89	15	100	45.1
8 (GOX)	4.22	5.1	0.365	0.492	260/280	2.87	20	400	25.7
1 (LOX)	——	——	0.222	0.31	435	2.51	8	250	66.8

[a]Grain length 102 in.

Table 5 Parameters used in frequency estimations for NASA Marshall Space Flight Center 11-in. hybrid motor tests

Test	$\bar{D}$, in.	L, in.	$\dot{m}_o$, lb/s	G_o, lb/in.$^2\cdot$ s	G_t, lb/in.$^2\cdot$ s	P_c, psi	O/F	f, Hz	ΔP_{osc}, %	τ_{bl2}, ms
3	3.4	102	3.44	0.38	0.527	745	2.6	6–10	15	67.1
4	4.3	102	3.36	0.23	0.325	325	2.4	10–20	20	47.8
6	3.7	102	8.36	0.78	1.024	750	3.2	10–15	12	34.0
7	5.3	102	3.41	0.15	0.22	335	2.1	6–15	15	73.9
8	5.7	102	3.87	0.15	0.209	850	2.6	2–5	60	193.4
9	6.1	102	6.34	0.28	0.392	215	2.6	6–20	33	26.1
15	5.4	108	10.20	0.45	0.599	1025	3.0	4	10	84.5
10	6.1	102	5.93	0.20	0.278	215	2.6	10–25	5	36.7

Table 6 Parameters used in frequency estimations for Arizona State University hybrid motor test

Parameter	Value
Test	1
D, in.	2.0
L, in.	27
$\dot{m}_o$, lb/s	3.44
G_o, lb/in.$^2\cdot$ s	0.29
P_c, psi	500
O/F	4.0
f, Hz	19
τ_{bl2}, ms	23.7

Note that Eqs. (10–12) are equivalent and that the constant multiplier c' is identical for all of these expressions.

The average temperature gas constant product that appears in the denominator of all of the boundary-layer delay time equations is assumed to be constant for all of the LOX/GOX motor tests that are considered in this paper. This is a fairly good assumption because RT is a weak function of the motor O/F for the practical operating conditions.[13] In fact, the maximum expected variation on the RT values for all of the LOX/GOX tests used for comparison is predicted to be less than 5%. The absolute value of RT_{av} is selected to be 6.38×10^5 m/s^2 for LOX/GOX motor tests, and because the same value is used for all calculations, any error in RT_{av} will only effect the numerical value of the empirical delay constant c'.

To double check the RT_{av} value used in the calculations, one could use the first acoustic frequency measured from the motor test data to estimate the speed of sound and, finally, RT_{av} based on the following equation.

$$f_{1-L} = \frac{\sqrt{\gamma RT_{\text{av}}}}{2L_m} \tag{13}$$

Here γ is the ratio of the specific heats averaged over the length of the motor, f_{1-L} is the first longitudinal acoustic mode, and L_m is the effective length of the motor. For a more accurate calculation, the complex gasdynamic model discussed in Refs. 13 and 20 can be used. All of the NASA Ames Research Center motor tests with 45-in. long grains had their first acoustic mode at around 370 Hz. For these tests with use of $\gamma = 1.25$ and $L_m = 1.27$ m, one obtains RT_{av} of 7.1×10^5 (m/s)^2, which is only 10% higher than the assumed value. RT_{av} for the N_2O test is selected to be 4.47×10^5 (m/s)^2. This is 30% lower than the RT_{av} for the GOX/LOX system due to the low temperature of the N_2O/hydrocarbon combustion products.

Table 7 Parameters used in frequency estimations for NASA Ames Research Center hybrid motor tests

Test	L, in.	G_o, lb/in.$^2\cdot$ s	P_c, psi	O/F	f, Hz	τ_{bl2}, ms
4F-4	32	0.44	528.0	3.97	41.6	13.6
4F-5	32	0.49	551.0	3.59	39.9	12.8
4F-1b	32	0.20	561.0	2.72	14.4	30.0
4F1-c	32	0.16	542.0	3.06	13.6	36.4
4P-01	45	0.39	318.0	2.69	40.8	12.4
4P-02	45	0.38	993.8	2.48	13.2	38.9
4P-03	45	0.40	939.1	2.65	14.4	35.9
4L-03	45	0.31	641.6	2.69	12.7	31.2
4L-04	45	0.52	656.7	2.66	23.6	19.0
4L-05	45	0.46	649.3	2.72	19.1	21.4
4L-08	45	0.44	525.0	2.64	23.3	18.0
4I-01	45	0.38	318.7	2.40	39.6	12.5
4P-04	45	0.21	159.1	1.73	42.4	10.8
4L-09	45	0.26	265.3	1.54	20.3	13.8
4L-10	45	0.43	590.0	2.89	27.0	18.4
4L-11	45	0.11	213.0	1.56	17.8	27.5
4L-12	45	0.13	301.0	2.01	15.54	32.5
4NF-01	45	0.39	602.2	2.77	22.60	23.3
4NF-02	45	0.22	600.4	2.34	11.10	40.7
4NF-03	45	0.36	500.8	2.96	23.20	21.6
4NF-04	45	0.48	568.5	3.01	32.75	18.2
4L-14	45	0.43	524.5	2.51	25.15	18.2
4ST-02	45	0.45	540.0	2.71	24.86	18.3
4L-15	45	0.31	555.5	2.09	14.94	26.4
4Rep-02	45	0.45	402.3	2.63	36.49	13.6

Now Eq. (7) can be coupled with the expressions for the boundary delay time to evaluate the frequencies predicted by the TCG coupled model,

$$f = 0.48 \frac{RT_{\text{av}}}{c'(V_p/V_m)[(1+\text{O/F})/(1+2\text{Q/F})]L^* c^*_{\text{exp}}} \tag{14a}$$

$$f = 0.48 \frac{(G_o + G_1)RT_{\text{av}}}{c'LP_c} = 0.48\left(2 + \frac{1}{\text{O/F}}\right)\frac{G_o RT_{\text{av}}}{c'LP_c} \tag{14b}$$

The oscillation frequency as a function of the boundary delay time predicted by the TCG coupled theory along with data from

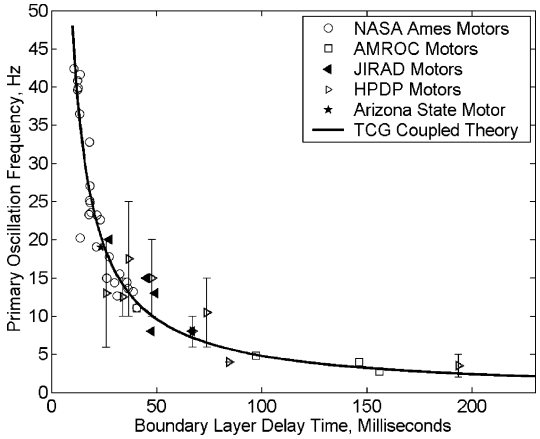

Fig. 13 Comparison of TCG coupled oscillation frequency prediction with hybrid motor test data available in the literature.

the hybrid motor development programs are shown in Fig. 13. Note that we have used a boundary-layer delay constant value c' of 2.050 for all motor tests to obtain the best fit between the theory and test results. Please note that this experimental value for c' is the same order of magnitude with the rough estimate, that is, $\sim$0.55, for a boundary layer with no blowing and no combustion.

When the wide range of test conditions is considered, the agreement between the measured pressure oscillation frequencies and the TCG coupled model predictions is surprisingly good. Note that the comparison includes 43 motor tests using results from four different development and research programs; using three separate oxidizers, that is, LOX, GOX and N_2O; covering a wide range of motor dimensions, that is, from 5 in. o.d. Arizona state motor up to 72 in. o.d. AMROC motor; using many different fuel compositions, that is, HTPB, HTPB/Escorez, and two paraffin-based formulations; and covering a wide range of operating conditions.

The average error between the frequencies predicted by the TCG coupled theory and the experimentally observed values is 13.94% for the all of the data shown in Fig. 13 other than the NASA test 4L-09, which clearly is an outlier. The errors associated with individual programs are 8.61% for NASA, 10.03% for AMROC, 19.37% for JIRAD, 29.68% for HPDP, and finally 13.94% for the nitrous motor test reported in Ref. 23. The maximum error is 41.96%, which corresponds to one of the HPDP motor tests.

A significant part of the difference between the observed and predicted frequencies is likely due to the inaccuracies associated with the reported frequencies and motor operating conditions in the literature. Note that the error in the operating conditions directly translates into the inaccuracies in the frequency estimation as can be seen from Eqs. (14a) and (14b). We believe that the most reliable data set is from the NASA motor tests because for these tests the low-frequency hybrid mode is carefully separated from the other modes of oscillation, that is, Helmholtz mode. This statement is supported by the fact that the NASA set has the least percent error compared to the data reduced from other programs. We believe that the most inaccurate set is from the HPDP motor tests, which reports the oscillation frequencies as a wide range as opposed to single peak values (Fig. 13). In fact, the combined error without the HPDP data improves to 10.30% with a maximum error of 29.04% for one of the JIRAD motor tests.

Equation (14a) indicates that, for motors operating at the similar O/F, the oscillation frequency is inversely proportional to the L^* of the motor. This conclusion is consistent with the previous results reported in the literature. Similarly, Eq. (14b), shows, for motors operating at equal oxidizer mass fluxes, chamber pressures, and O/F, the oscillation frequency decreases with increasing fuel grain length. To prove that motor length plays a critical role setting the oscillation frequency, we have plotted the NASA Ames Research Center motor data, which contains two sets of grain lengths, by removing the length effect from the scaling law. This resulted in an increase in the scatter in the frequency data, indicating the importance of the grain length. A similar check to confirm the importance of length can be conducted by comparing the JIRAD and HPDP motor tests, that is, ran with grains 102 in. long, with the NASA Ames Research Center paraffin tests, that is, ran with grains 32 or 45 in. long, that were conducted under very similar operating conditions. For example, comparing test 8 of the HPDP program to paraffin-based motor test 4P-01 shows that grain length must be included in the scaling law to explain the discrepancy in the oscillation frequencies for these tests. The same conclusion can be drawn by comparing test 2 of HPDP program to the NASA Ames Research Center test 4L-08.

TCG coupled theory predicts oscillations of the regression rate/fuel mass generation rate and would be observed directly in a hybrid motor as the radial oscillations of the diffusion flame within the boundary layer. The gasdynamic model converts the fuel mass generation rate oscillations to the chamber pressure oscillations. It is expected that a system operating at higher O/F ratios would produce less chamber pressure oscillations because fuel mass constitute a smaller fraction of the total mass expelled from the nozzle. This fact is observed in NASA Ames Research Center motor tests, namely, high O/F motors, in general, presented lower amplitudes chamber pressure oscillations compared to the mean chamber pressure.

The simple linear model presented in this paper successfully explains the generation of small-amplitude, low-frequency oscillations and the scaling of the frequency. However, it also falsely predicts an indefinite growth of chamber pressure oscillations. In reality, the nonlinear mechanisms that exist in a hybrid motor would limit the indefinite growth of the oscillations and result in limit-cycle oscillations that are commonly observed in motor tests. Moreover, the simple theory does not explain when these low-frequency instabilities will take place and what their amplitudes would be. It has been shown in the hybrid development programs that the fore end configuration/volume of the motor plays an important role in setting the amplitude of the low-frequency instabilities. The motor tests indicated that, at least for gaseous motors, axial injectors result in more stable operation compared to the radial or conical injection of the oxidizer.

A natural explanation for these observations is that the TCG coupled instability mechanism almost always exist in hybrid systems, but the amplitude of the limit-cycle oscillations will depend on the excitation level by the disturbances in the right frequency range. We believe that the fore end fluid dynamics, that is, vortex shedding, is the primary source of disturbances in a hybrid rocket. For example, changing the injection scheme of the oxidizer from axial to radial may introduce a flow disturbance component that is preferred by the TCG coupled system. If one assumes that all of the low-frequency oscillations are developed by the fluid mechanics at the fore end of the motor, one would fail to explain the length effect on the oscillation frequency. Also all oxidizer injection schemes under identical motor operating conditions seem to produce the same oscillation frequency. This fact is also difficult to explain by the assumptions that all of the oscillations are produced from the fluid dynamic events at the fore end of the motor because the injection scheme should alter the fluid mechanics significantly, that is, vortex shedding frequency.

Note that most musical instruments also work on the same principle.[24] For example, in a flue organ pipe the column of air inside the pipe is set into vibration, that is, at its natural frequencies, by an edge tone that is produced by a jet of air that impinges on a carefully designed lip. The vortex shedding at the lip sets the edge tone, which itself excites the natural modes in the pipe. Note that in the case of an organ pipe the jet speed and the lip geometry is carefully selected for the pipe length such that the edge tone produced at the lip contains a large component at the natural frequency of the pipe that needs to be excited. In this organ pipe analog, the lip is the fore end of the motor, that is, geometry, injection scheme, velocity, etc., and the organ pipe is the hybrid system modeled by the TCG coupled theory.

Conclusions

The following conclusions can be drawn from the results of the TCG coupled model.

1) A plausible mechanism that generates low-frequency chamber pressure oscillations is suggested. This mechanism is due to the coupling of the thermal lags, the gas-phase combustion, and gasdynamic subsystems of the hybrid rocket. The physical transient model of the motor is presented in a mathematical formalism that allows one to estimate the expected oscillation frequency. The amplitude of the oscillations can not be determined by this linear model.

2) The oscillation frequency estimated by the model is in very good agreement with the motor test data from several programs utilizing three distinct oxidizers, several fuel formulations, and a wide range of motor dimensions and operating conditions. We suggest the following equation as a universal scaling law for the primary hybrid oscillation frequency:

$$f = 0.2341\left(2 + \frac{1}{\mathrm{O/F}}\right)\frac{G_o R T_{\mathrm{av}}}{L P_c} \tag{15}$$

where $RT_{\mathrm{av}} = 6.38 \times 10^5$ (m/s)^2 for GOX/LOX systems and $RT_{\mathrm{av}} = 4.47 \times 10^5$ (m/s)^2 for low-energy oxidizer systems such as N_2O.

3) This mode of instability is common to all kinds of hybrids: liquefying or conventional fuels, liquid oxidizer or gaseous oxidizers. It is reasonable to believe that this low-frequency mode is present in every hybrid system to some extent. Some motors are more unstable compared to the others because these motors do possess more disturbances to excite the TCG-coupled oscillations. For example, the oxidizer injector configuration or precombustion chamber geometry affects the scale and the frequency of the disturbances that would excite the commonly observed low-frequency mode. For this reason, the design of the fore end of the motor has been critical in controlling the stability of the system.

4) Even though the linear theory very successfully predicts the oscillation frequency of the chamber pressure, it fails to establish an estimation process for the amplitude of the oscillations. The theory predicts an unlimited growth of the oscillations. In reality, the amplitude of the chamber pressure fluctuations will be limited by nonlinear effects that are not covered in the linearized TCG-coupled theory.

5) It has been shown that the longitudinal acoustic oscillations that are commonly coexist with the low-frequency oscillations can be generated by the excitation induced by the nonlinear waveforms of the low-frequency chamber disturbances. In short, it is plausible that high-frequency acoustic modes are driven by the low-frequency oscillations.

Estimating the amplitude of the pressure oscillations and developing schemes to minimize (and eventually eliminate) them is one of the most important practical aspects of a stability theory. Thus, one of the key directions for future research is to extend the theory to account for the nonlinear phenomena that takes place in the motor and to better understand the dynamic interactions between the fundamental hybrid combustion scheme and the disturbances that excite the instability modes. Another area of interest is to develop the feed system and the oxidizer atomization/vaporization models and to integrate them with the existing TCG-coupled system to predict the transient behavior of a liquid-fed hybrid rocket. Finally, it would be desirable to modify the transient theory to understand the effects of variations on the classical hybrid scheme. Two of these promising schemes are the hybrid systems utilizing nano-sized metal powders as fuel additives and systems with high-intensity swirl injection of the oxidizer. Both of these variations change the hybrid combustion process to some extent, and it is expected that they would also alter the stability character of the combustion system.

Acknowledgments

Part of this work was carried out under Cooperative Agreements NAG3-2615 with the NASA John H. Glenn Research Center and Agreements NCC2-1172 and NCC2-1300 with the NASA Ames Research Center.

References

[1]Beckstead, M. W., and Price, E. W., "Nonacoustic Combustion Instability," *AIAA Journal*, Vol. 5, No. 11, 1967, p. 1989.

[2]Brown, R. S., and Muzzy, R. J., "Linear and Nonlinear Pressure Coupled Instability of Solid Propellants," *AIAA Journal*, Vol. 8, No. 8, 1970, p. 1492.

[3]Culick, F. E. C., and Yang, V., *Combustion Instabilities in Liquid Rockets*, Progress in Astronautics and Aeronautics, Vol. 169, AIAA, Washington, DC, 1995, pp. 3–37.

[4]Guthrie, D. M., and Wolf, R. S., "Non-Acoustic Combustion Instability in Hybrid Rocket Motors," Rept. N 91-24250, Camarillo, CA, 1991.

[5]Boardman, T. A., Carpenter, R. L., and Claflin, S. E., "A Comperative study of the Effects of Liquid- Versus Gaseous-Oxygen Injection on Combustion Stability in 11-inch-Diameter Hybrid Motors," AIAA Paper 97-2936, July 1997.

[6]De Zilwa, S., Arif Karabeyoglu, M., and Zilliac, G., "Combustion Oscillations in High Regression Rate Hybrid Rockets," AIAA Paper 2003-4465, July 2003.

[7]Greiner, B., and Frederick, R. A., Jr., "Experimental Investigation of Labscale Hybrid Instability," AIAA Paper 94-2878, June 1994.

[8]Boardman, T. A., Brinton, D. H., Carpenter, R. L., and Zolods, T. F., "An Experimental Investigation of Pressure Oscillations and Their Suppression in Subscale Hybrid Rocket Motors," AIAA Paper 95-2689, July 1995.

[9]Jenkins, R. M., and Cook, J. R., "A Preliminary Analysis of Low Frequency Pressure Oscillations in Hybrid Rocket Motors," AIAA Paper 95-2690, July 1995.

[10]Greiner, B., and Frederick, R. A., Jr., "Hybrid Rocket Instability," AIAA Paper 93-2553, June 1993.

[11]Wooldridge, C., Marxman, G. A., and Kier, R., "Investigation of Combustion Instability in Hybrid Rockets," NASA CR-66812 Final Rept., Oct. 1969.

[12]Wooldridge, C., and Marxman, G. A., "Combustion Instability and the Role of Chemical Kinetics in Hybrid Combustion," AIAA Paper 68-498, June 1968.

[13]Karabeyoglu, M. A., "Transient Combustion in Hybrid Rockets," Ph.D. Dissertation, Dept. of Aeronautics and Astronautics, Stanford Univ., Stanford, CA, Aug. 1998.

[14]Karabeyoglu, M. A., and Altman, D., "Dynamic Modeling of Hybrid Rocket Combustion," *Journal of Propulsion and Power*, Vol. 15, No. 4, 1999, pp. 562–571.

[15]Marxman, G. A., Wooldridge, C. E., and Muzzy, R. J., *Fundamentals of Hybrid Boundary Layer Combustion*, Progress in Astronautics and Aeronautics, Vol. 15, Academic Press, New York, 1964, pp. 485–522.

[16]Parikh, P. G., Jayaraman, R., Reynolds, W. C., and Carr, L. W., *Transient Response of a Turbulent Boundary Layer*, FED-Vol 12, American Society of Mechanical Engineers, New York, 1984, p. 31.

[17]Schlichting, H., *Boundary Layer Theory*, McGraw–Hill, New York, 1955, Chap. 21.

[18]Moelwyn-Hughes, E. A., *Physical Chemistry*, 2nd rev. ed., Pergamon, Oxford, 1961, Chap. 6.

[19]Altman, D., and Humble, R., "Hybrid Rocket Propulsion Systems," *Space Propulsion Analysis and Design*, McGraw–Hill, New York, 1995, p. 382.

[20]Karabeyoglu, M. A., De Zilwa, S., Cantwell, B. J., and Zilliac, G., "Transient Modeling of Hybrid Rocket Low Frequency Instabilities," AIAA Paper 2003-4463, July 2003.

[21]Karabeyoglu, M. A., Zilliac, G., Cantwell, B. J., De Zilwa, S., and Castellucci, P., "Scale-up Tests of High Regression Rate Liquefying Hybrid Rocket Fuels," AIAA Paper 2003-1162, Jan. 2003.

[22]Boardman, T. A., Carpenter, R. L., Goldberg, B. E., and Shaeffer, C. W., "Development and Testing of 11- and 24-Inch Hybrid Motors Under the Joint Government/Industry IR&D Program," AIAA Paper 93-2552, June 1993.

[23]Pucci, J. M., "The Effects of Swirl Injector Design on Hybrid Flame-Holding Combustion Instability," AIAA Paper 2002-3578, July 2002.

[24]Jeans, J., *Science and Music*, Dover, New York, 1968, Chap. 4.